The mechanism of ligand-induced chiral transmission through a top-down selective domain etching process

Junjie Hao, Junzi Li, Meijuan Chen, Xijian Duan, Bing Xu, Yiwen Li, Tingchao He, Xiao Wei Sun, Marie-Hélène Delville, Jiaji Cheng

▶ **To cite this version:**

Junjie Hao, Junzi Li, Meijuan Chen, Xijian Duan, Bing Xu, et al.. The mechanism of ligand-induced chiral transmission through a top-down selective domain etching process. Materials Chemistry Frontiers, 2022, 6 (9), pp.1194-1208. 10.1039/D2QM00075J . hal-03660762

HAL Id: hal-03660762
https://hal.science/hal-03660762

Submitted on 6 May 2022

HAL is a multi-disciplinary open access archive for the deposit and dissemination of scientific research documents, whether they are published or not. The documents may come from teaching and research institutions in France or abroad, or from public or private research centers.

L'archive ouverte pluridisciplinaire **HAL**, est destinée au dépôt et à la diffusion de documents scientifiques de niveau recherche, publiés ou non, émanant des établissements d'enseignement et de recherche français ou étrangers, des laboratoires publics ou privés.

Please do not adjust margins

ARTICLE

Mechanism of Ligand-Induced Chiral Transmission Through a Top-Down Selective Domain Etching

Junjie Hao,[1,2,#] Junzi Li,[3#] Meijuan Chen,[2,4] Xijian Duan,[2,5,6] Bing Xu,[6] Yiwen Li,[4] Tingchao He,[3*] Xiao Wei Sun,[2,5,6*] Marie-Hélène Delville,[1*] Jiaji Cheng[4*]

DOI: 10.1039/D2QM00075J

Induced chirality in colloidal semiconductor nanoparticles has received much attention in the past few years as an extremely sensitive spectroscopic tool and because of the promising applications of chiral quantum dots (QDs) in sensing, quantum optics, and spintronics. Yet, the origin of the chiroptical effects induced in these nanoparticles is not fully understood, partly because almost all theoretical and experimental studies performed so far are based on the comparison of the g-factor of bulk solutions, which may not truly reflect the variation of the chiral signal in a single nanoparticle. This is because, at a given absorbance value, any change in the molar absorption coefficient at the single nanoparticle level does seriously affect the estimation of the real number of nanoparticles and comparison in-between solutions. Here, we show that using a top-down chemical etching of colloidal two-component CdSe/CdS dot-in-rods (DRs) nanoparticles can facilitate precise control of nanocrystals solutions with identical concentrations, which cannot be achieved by bottom-up hot injection technology alone. This approach is highly required for studying ligand-induced chiral conduction mechanisms because it effectively eliminates the influence of both the concentration of nanoparticles and ligands at the same time, instead of relying only on the g-factor related to absorbance. Results showed, thanks to the top-down selective domain etching system, that the shell layer had a negative correlation with the chirality of the first exciton peak (CdSe core contribution), but a positive correlation with the chirality of the CdS shell absorption. At the same time, the core integrity is crucial for DRs to maintain high CD and CPL signals. This work, on the one hand, advances the understanding of the fundamental origin of chiral conduction effects induced in semiconductor nanoparticles, and on the other hand, opens a path to applications using chiral materials.

Introduction

Chiral semiconducting quantum dots (SQDs) form an emerging field in nanomaterials, with potential applications in asymmetric catalysis,[1] bio-sensing,[2, 3] chiral recognition,[4, 5] and as circularly polarized light sources,[6, 7] attributed to the coupling of chirality with their inherent photoluminescence (PL) and optical activity. Chirality of QDs can be achieved by several methods,[8-11] but ligand-induced chirality is the most common and widely used. It is based on the principle that a strongly induced chirality in the aqueous phase can simply be obtained by replacing the originally achiral ligands present on the semiconductor nanoparticles while in the organic phase with a water-soluble chiral ligand (e.g. cysteine).[10, 12-16] Moreover, various studies have shown a complex evolution of circular dichroism (CD) spectra with the QD size and composition.[12, 17] CD was found to be dependent on the surface-to-volume ratio,[18, 19] the shell thickness,[5, 17] or the absorption ratio of shell-to-core (ARSC).[10]

Two chirality-related research methodological approaches have been used to study the mechanism of induced chirality. The first is to study the chiral conduction mechanism by varying the ligands.[20-24] It investigates the different binding strengths of the ligands and the distances between the chiral centre and the different binding sites, to rationalize the behaviour and set up a mechanism of chirality induced by different chiral molecules. The other route is mainly based on a bottom-up colloidal process that involves comparing several series of nanoparticle preparations to study the mechanism of action, looking at different sizes,[5, 12] different shapes,[10, 25-28] different shell-thicknesses,[5, 17, 29] and self-assemblies.[11, 30, 31] However, the precise control of the different morphologies especially the

[1] CNRS, Univ. Bordeaux, Bordeaux INP, ICMCB, UMR 5026, Pessac, F-33608, France;
[2] Key Laboratory of Energy Conversion and Storage Technologies (Southern University of Science and Technology), Ministry of Education, Shenzhen 518055, China;
[3] College of Physics and Optoelectronic Engineering, Shenzhen University, Shenzhen, Guangdong 518060, China;
[4] School of Materials Science and Engineering, Hubei University, Wuhan, Hubei 430062, China;
[5] Guangdong University Key Laboratory for Advanced Quantum Dot Displays and Lighting, Guangdong-Hong Kong-Macao Joint Laboratory for Photonic-Thermal-Electrical Energy Materials and Devices, Shenzhen Key Laboratory for Advanced Quantum Dot Displays and Lighting, SUSTech-HUAWEI Joint Lab for Photonics Industry, and Department of Electrical and Electronic Engineering, Southern University of Science and Technology, Shenzhen 518055, China;
[6] Shenzhen Planck Innovation Technologies Co. Ltd., Shenzhen 518055, China.
# These authors contributed equally to this work.
Email: jiajicheng@hubu.edu.cn; marie-helene.delville@icmcb.cnrs.fr; sunxw@sustech.edu.cn; tche@szu.edu.cn
† Footnotes relating to the title and/or authors should appear here.
Electronic Supplementary Information (ESI) available: [details of any supplementary information available should be included here]. See DOI: 10.1039/x0xx00000x

Please do not adjust margins

dimensions of the anisotropic NCs such as the width and length of DRs, under kinetic growth conditions, remains quite challenging because the reaction does not proceed toward a desired single (thermodynamically stable) endpoint.[32] Therefore, as the kinetic growth proceeds, uncontrollable structural aspects increase: the size distribution of anisotropic NCs broadens, resulting in little control over their optical properties, such as emission wavelengths and bandwidths. Furthermore, the relative extinction coefficient per mole of particles is highly dependent on the volume of the NCs, whether it is a single NC or a core-shell NC such as CdSe/CdS.[33, 34] Thus, the conventional g-factor is not enough to characterize the chiral signal evolution of a single nanoparticle, because it just eliminates the effect of absorbance from the CD signals.

For a given value of the absorbance, as the molar absorption coefficient of NPs increases, the number of particles decreases, *i.e.,* the number of nanoparticles contributing to the g-factor decrease. Therefore, in a system with a large change in the molar absorption coefficient (such as different shell volumes of CdSe/CdS NCs), it is not possible to simply compare the variation in the g-factor to access the chiral properties of an individual nanoparticle, since the observed chiral evolution may represent the convolution of different morphologies. For instance, in the same CdSe/CdS core-shell QDs system, two kinds of g-factor evolutions appear in different research groups (they first increased (1 to 3 MLs) and then decreased,[5] or gradually decreased[17]). Therefore, it is very important to study the mechanism of the generation of chirality in single nanoparticles. The control of different morphologies at the same concentration is difficult to achieve only by bottom-up colloidal hot injection technology because the reaction yield and purification efficiency are difficult to control and cannot be simply considered as giving the same concentration as that of the core. On the other hand, to calculate the concentration of the composite semiconductor NCs, the full use of various characterization methods, such as TGA, XPS, TEM, etc., must be combined. However, this strategy is hampered by the fact that the calculation of the molar concentration of core-shell nanocrystals requires a large number of nanocrystals (usually tens of milligrams for TGA), which is difficult to achieve due to the small amounts of products and their high cost. In particular, for the preparation of anisotropic nanocrystals, such as CdSe/CdS DRs (with a high chiral signal compared to other morphologies),[10, 28, 35] which requires expensive reagents such as n-octadecyl phosphonic acid (ODPA), n-hexyl phosphonic acid (HPA), tri-n-octyl phosphine oxide (TOP), etc., Therefore, it is very important to find a low-cost and controllable method to prepare samples with the same concentration.

Top-down etching of colloidally grown nanocrystals provides a versatile tool for shaping the structure of a series of comparative experiments starting with the same stock solution. The inorganic core can be oxidized, etched, and even completely dissolved, which normally defeats the function of the original nanocrystal/ligand complexes.[36] Several groups have reported the modification of structural and optical properties of as-grown NCs by top-down etching processes. Peng *et al.* successfully used this method to study the size evolution of the NPs and the absorption of the first exciton peak. Their results greatly simplified the study of QDs, and the particle size could be calculated by a simple UV-vis. test instead of TEM, which is of great significance.[37] On the other hand, due to the chemical or photooxidative dissolution of surface atoms, top-down etching technology has been successfully used in semiconductors to tune the size of binary nanocrystals and to study the interface of dots or peanut-shaped core-shell QDs. For instance, shape control by etching has been reported for several semiconductor nanostructures, CdX,[37-40] PbS,[41] InP,[42] binary nanocrystals or CdSe/CdS,[43] CdSe/CdTe,[44, 45] CdSe/ZnS/CdSe[46] core-shell NCs.

Based on the apparent potential of the top-down etch-based methods in nanoparticle synthesis, we propose herein a technique that uses the same type of cores and obtains different core-shell DRs structures by top-down etching techniques to study the ligand-induced chiral transfer mechanism. The method is illustrated by performing isotropic etching of colloidal nanostructures consisting of two spatially asymmetric material domains. Furthermore, this etching method relies on the irreversible etching of chalcogenides in a controlled way by a benzoyl peroxide solution.[44-46] The top-down etching process of CdSe/CdS DRs monitored *in situ* by UV-vis. spectrometry can be divided into two steps: First, a slow isotropic etching process takes place only at the CdS shell level, because of the complete protection of the CdSe core. The chemical etching of the CdSe/CdS dot-in-rod (DRs) structures promotes a partial dissolution of the CdS shell from the surface of the CdSe dots, which induces an increased chiral signal for the single-particle when modified with chiral molecules. In the second step, after further etching of the CdS shell, the CdSe core is gradually exposed, and a faster etching process begins. This is due to the different oxidation activities of the two chalcogenides.[45] By controlling the top-down etching and ligand exchange processes, we can achieve the comparison of nanoparticle solutions of identical concentration, *i.e.,* we have access to the chiral signal of a single particle, and they can be compared. In particular, with this special etching process, we can further analyze the reason why the DRs structure has a high chiral signal. As shown in the references, the chirality of CdSe/CdS DRs[10, 35] is significantly higher than that of CdSe or CdS QDs respectively.[5, 20] In the second stage, since the shell cannot completely protect the CdSe core, the defects of the core increase, which may affect the conduction of electrons and holes between the core and the shell explaining the sharp decrease of the chiral signal during the CdSe core etching. The novelty of this top-down etching is that it allows fine-tuning of the quantum confinement dimension or quantum size effect of NCs in solutions of the same concentration. In this sense, etching seems to be the most natural and potentially the easiest way to study the evolution process of the chiral signal of a single particle. These results suggest that the greatest capacity of the etching approach is anticipated for the application of this technique to multi-domain nanocrystals, where it may lead to new chiral signals that are inaccessible by conventional colloidal methods.

Results and discussion,

To evaluate the ligand-induced chirality of NPs, the CD anisotropy factor (also known as Kuhn's dissymmetry ratio, (g) is used for comparison and to explore the mechanism in most of literature papers.[10, 12, 14, 17, 25-27, 47] The CD anisotropy factor is defined as $g = \Delta\varepsilon/\varepsilon = (A_L - A_R)/A = \theta/(32980 \times A)$, where A is the conventional absorbance of non-polarized light, θ with the unit of mdeg is the ordinate of CD spectrum, and A_L and A_R are the absorptions of left and right circularly polarized light, respectively.[12] The CD anisotropy factor g is claimed independent of the concentration and the path length if the CD and absorbance spectra are taken from the same sample. However, the absorbance at different wavelengths varies greatly, especially for the core-shell nanocrystals (NCs) with large "effective Stokes-shift" (a large wavelength gap between excitation and emission spectra).[48-50] For instance, in the CdSe/CdS dot-in-rods (DRs) samples, the value of the absorption ratio of shell-to-core (ARSC) changes by more than 12 times in different comparison samples, and in many cases, the ARSC is higher than 10.[10] Due to the large molar absorptivity change in the CdS shell absorbance, based on Beer Lambert's law, the number of nanoparticles does change dramatically for a given value of the absorbance. In this case, if only the g-factor is used to study the evolution of the chiral signal, especially for a single nanoparticle, results can be contradictory [5, 17] and the true change law may be hidden. Furthermore, due to the difference in absorbance and the Cd and CdSe regions and the sensitivity of the CD spectra, we managed to control the concentrations of nanoparticles to achieve close ODs, and analyse the chiral signals in both wavelength ranges.[51]

Characterization of the single DRs

To explore the ligand-induced chirality variation, we then use this top-down etching method to provide a series of NCs solutions, all with the same concentration, so that the chirality analysis of individual nanoparticles becomes possible just by the ordinate of CD spectra (θ), which excludes the influence of alterations in concentration and absorbance on the exploration of the chiral mechanism. It should be pointed out that the anisotropic g-factor at the first excitonic transition shows a 10-fold enhancement as the shape changes from spherical QDs to one-dimensional quantum rods (QRs),[27] and these excellent high chiral signals are displayed in both the core (500-700 nm) and the shell (< 500 nm) of the CdSe/CdS dot-in-rod (DRs).[10, 35] We, therefore, chose the CdSe/CdS DRs system for this top-down etching study.

The synthesis conditions of these DRs are the same as already published;[10, 52] CdSe/CdS DRs with different shell-thicknesses were obtained by varying the injection temperature, for instance, the thin shell is obtained at 593 K (see experimental part). To show the universality of the etching experiment, three CdSe cores with different emissions (yellow, orange, and red) were used (Figure S1 and Table S1). Their FWHM can be maintained at around 30 nm, indicating that they are good in size uniformity.

DRs with different shell thicknesses were obtained by varying the temperature as shown in Figure 1, Figure 2, and Table 1. The shell thickness was three monolayers (3ML) (DR-1), two monolayers (2ML) (DR-2), and one monolayer (1ML) (DR-3), respectively. The average thickness of one monolayer of CdS was taken as 0.35nm, so one additional layer growth would increase the diameter of a nanocrystal by 0.7 nm.[53] As shown in Figure 2, after the first exciton peak is normalized, the absorption below 500 nm corresponding to the CdS shell sharply increases with its thickness, and the PL emission is simultaneously red-shifted with the absorption peak. This is due to the CdS shell which cannot provide potential barriers that are large enough to prevent the leakage of the exciton into the shell.[54] Surprisingly, the FWHM of CdSe/CdS DRs PL is reduced to 23 nm, (Table 1) a narrower value than that of the CdSe core (Table S1).

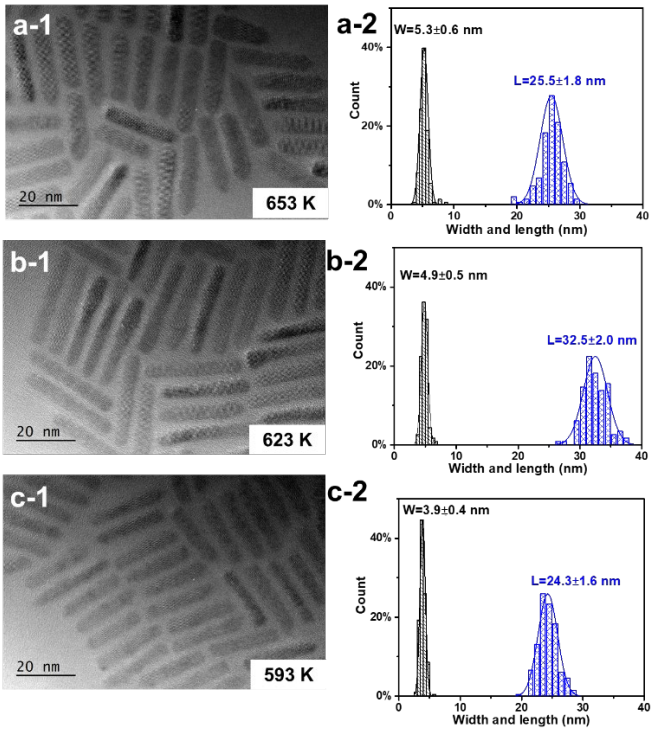

Figure 1. TEM images of DRs with different shell thicknesses: (a) DR-1, three monolayers (3ML); (b) DR-2, two monolayers (2ML); (c) DR-3, one monolayer (1ML).

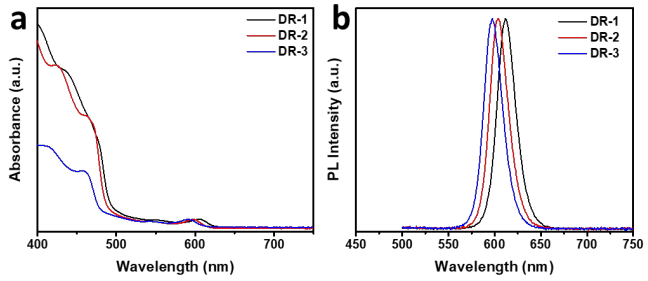

Figure 2. a) The UV-vis. spectra with absorbance was normalized at 600 nm of the different synthesized under different reaction conditions; b) PL of the same DRs.

Please do not adjust margins

These CdSe/CdS DRs etched or not were transferred to a water solution containing the L- or D- cysteine solution (0.2 mol/L, 2 mL), and the reaction mixture was deoxygenated and stirred at room temperature under argon in the absence of light for 24 h to obtain the chiral DRs. Benzoyl peroxide was used to etch them in a controlled way in the presence of a large excess of benzylamine in solution to study their chiral evolution.[43]

Table 1. Physical characterizations of the different CdSe/CdS DRs.

	Core Diam. (nm) [a]	Diam. (nm)	Length (nm)	PL (nm)	FWHM (nm)	QY (%)	Abs (nm)
DR-1	3.2	5.3±0.6	25.5±1.8	612	23	61	605
DR-2	3.2	4.9±0.5	32.5±2.0	604	23	40	597
DR-3	3.2	3.9±0.4	24.3±1.6	597	23	41	591
DR-4	3.9	4.2±0.4	23.9±2.5	620	23	55.5	613
DR-5	4.7	4.9±0.6	17.5±1.7	631	24	41	623

[a] Diameter of the CdSe core is determined from the absorption spectrum by Peng's equation (nm).[37]

Ideally, such a controlled top-down etching process indicates that the overall size distribution of the DRs should not change significantly, although the shell thickness of the DRs decreases with time. Experimentally, the surface ligands of the nanocrystals were exchanged from ODPA/TOPO to benzylamine to allow improving the reproducibility of the etching procedure. Indeed, as mentioned by Khon,[43] the benzylamine molecules in this case partly replace the facet-selective HPA and TOP ligands at the DRs surface that may potentially promote different etching rates.

The rigid and short tail of benzylamine, in comparison to the long and flexible hydrocarbon chain of ODPA/TOPO, made the etching process more efficient. The top-down etching process (*in situ* monitored by UV-vis. absorption) can be performed as many times as wanted;[46] the CD spectra of exciton region of (3ML) DR-1 samples and those of samples etched one and two times, are for example presented in Figure 3, (they correspond to the excitonic bands of in the DR-1 UV-vis. spectrum (Figure S2d)).

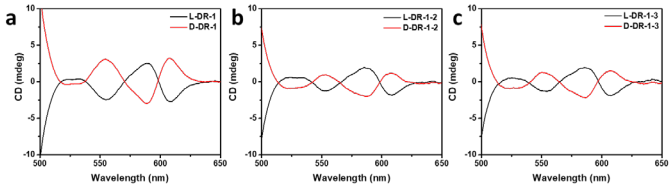

Figure 2. CD spectra evolution of DR-1 at the first exciton absorption peak during the etching process. (a) CD spectrum of benzylamine-modified DR-1-1 after Cys exchange and no etching; (b) CD spectrum of DR-1-2 after one etching cycle and Cys exchange; (c) CD spectrum of DR-1-3 after two etching cycles and Cys exchange.

As expected, the CD spectra split at the absorption excitonic maxima, crossing zero and changing sign, a behaviour characteristic of the "Cotton effect" in chiro-optical spectra.[55] This has been assigned to the splitting of the excitonic hole level (valence band) due to coupling interactions with the HOMO of the cysteine ligand producing two sub-bands, which are preferentially excited by alternating circular polarizations, though at present the precise mechanism of this coupling is not clear.[5] The corresponding g-factors are given in Table 2 and shown in Figure S2.

As shown in Figure 3, as the etching proceeds and the shell layer decreases, the CD signal of single DRs increases at the first exciton absorption peak (~ 600 nm, response of the signal of core), following the same trend as the g-factor (Figure S2, Figure S3 and Table 2). This is consistent with the literature:[17] the chemical etching of CdSe/CdS DRs promotes a partial dissolution of the CdS shell from the surface, which allows for a CdSe domain to come into closer contact with the surrounding chiral ligands and increase the chirality *via* more direct interaction with the core.

Table 2. The CD and g-factor of L-Cys-DR-1-n at the first exciton absorption peak during the etching process (n = 1-3).

DR-1-	UV-vis (nm)	CD^+/λ_{CD} [a]	CD^-/λ_{CD} [b]	$\lvert CD^+ - CD^- \rvert/2$ [c]	g_{CD+}/λ_{CD} [d]	g_{CD-}/λ_{CD} [e]	$\lvert g_{CD+} - g_{CD-} \rvert/2$ [f]
1	602.5	1.787/ 590.6	-1.295/ 608.2	1.541	0.787/ 588.2	-0.572/ 611.6	0.680
2	601.4	1.930/ 586.0	-1.827/ 608.2	1.879	1.002/ 585.2	-0.847/ 611.8	0.925
3	600.2	1.944/ 585.6	-1.895/ 608.0	1.920	1.085/ 582.8	-1.032/ 614.0	1.059

[a, b] CD anisotropy at the most intense positive and negative CD bands (mdeg/nm), [c] magnitude of the CD signal, defined as $|CD^+ - CD^-|/2$, [d, e] CD anisotropy g_{CD}- factors at the most intense positive and negative CD bands (10^{-4}/nm), [f] Magnitude of the g_{CD} factor, defined as $|g_{CD+} - g_{CD-}|/2$ (10^{-4}/nm).

Considering that (i) the total amount of DRs in solution does not change during the controlled etching experiments, that (ii) we also control the corresponding absorbance during the Cys ligand exchange process just by using the same amount of Cys (0.1 M, 2 ml), then the CD intensity shown in Figure 3 can be assumed to directly reflect the chiral properties per mole of particles. Even if we do not know the specific number of DRs, the concentration of nanoparticles can be controlled by UV-vis. absorption monitoring. This explains the minor change in the absorption intensities of the CdSe cores in single DRs and the nice reproducibility during the etching process (Figure S2d), the g-factor in the bulk solution representing also the evolution of the chiral signal of the single-particle.

When focusing on the range of 350-500 nm corresponding to the CD signals of the CdS shell, the chiral signals are much more intense, and results can become complicated. Indeed, in this case, the g-factor first increases and then decreases, while, the CD signal of these solutions of the same concentration of NPs gradually weakens (Table 3, Figure 4, Figure 5, and Figure S4).

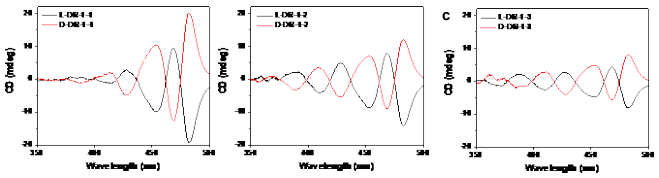

Figure 3. CD spectrum variations of DR-1 (< 500 nm) during the etching process. a) CD spectrum of benzyl amine-modified DR-1-1 after Cys exchange; b) CD spectrum of DR-1-2 after one etching cycle and Cys exchange; c) The CD spectrum of DR-1-3

after two etching cycles and Cys exchange. The concentration is 5 times lower than in Figure 3 and Figure S2.

Table 3. The CD and g-factor of L-Cys-DR-1-n (n = 1-3) (350-500 nm) during the etching process.

DR-1-	UV-vis. (nm) (core)	CD^+/λ_{CD}[a]	CD^-/λ_{CD}[b]	$\lvert CD^+ - CD^- \rvert/2$[c]	g_{CD+}/λ_{CD}[d]	g_{CD-}/λ_{CD}[e]	$\lvert g_{CD+} - g_{CD-} \rvert/2$[f]
1	602.5	9.596/ 468.7	-19.296/ 482.3	14.446	1.204/ 469.0	-4.231/ 485.2	2.718
2	601.4	7.888/ 468.9	-14.205/ 482.6	11.047	1.367/ 468.9	-4.555/ 485.8	2.961
3	600.2	4.282/ 468.1	-8.143/ 482.5	6.213	0.996/ 468.6	-3.566/ 485.8	2.281

[a, b] CD anisotropy at the most intense positive and negative CD bands (mdeg/nm), [c] magnitude of the CD signal, defined as $\lvert CD^+ - CD^- \rvert/2$, [d, e] CD anisotropy g_{CD} -factors at the most intense positive and negative CD bands (10^{-4}/nm), [f] magnitude of the g_{CD} factor, defined as $\lvert g_{CD}^+ - g_{CD}^- \rvert/2$ (10^{-4}/nm).

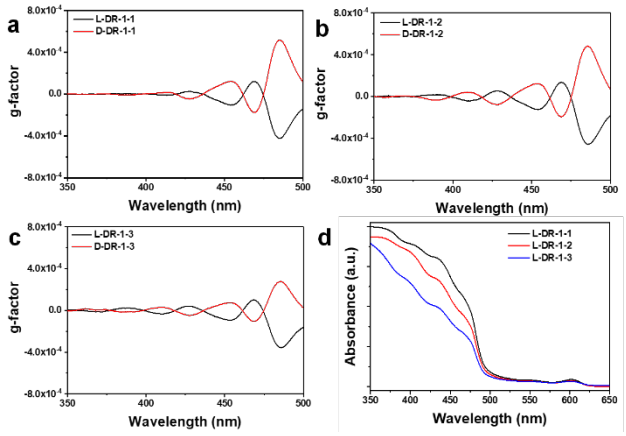

Figure 4. g-factor variations and corresponding UV-vis. Spectra of DR-1-n (350-500 nm) as shown in Figure 4. (a) CD spectrum of the benzylamine-modified DR-1-1 after Cys exchange, (b) CD spectrum of DR-1-2 after one etching cycle and Cys exchange, (c) CD spectrum of DR-1-3 after two etching cycles and Cys exchange, (d) corresponding UV-vis. Absorption spectra of the different etching samples. The concentration is 5 times lower than in Figure 3 and Figure S2 so that the absorbance around 480 nm is maintained below 2.

The volume of the CdS shell indeed decreases with the shell etching, providing a reduced available surface area for the ligand binding, thereby reducing the chiral signal provided by the shell. Additionally, this very same decrease in the shell volume induces a significant change in the absorption in the 350-500 nm range (Figure 5d and Figure S4) so that in this wavelength range, the CD and the g-factor of a single nanoparticle evolve in opposite ways. CD gradually decreases, while the g-factor increases first and then decreases because the absorption is not constant anymore (See Figure S4). As a result, this is one of the reasons for the complicated behaviours observed in chiral changes, which shows that access to the chirality of a single particle is required. Here, we demonstrate that such a top-down chemical etching of semiconductor nanocrystals can represent a powerful tool to reduce the difficulty in analysing comparative experiments, resulting in the improvement of the operability of the experiment. The constancy in the intensity of the CdSe absorption band provides a real opportunity to study the variation of chirality at the scale of a single NR since the number of NRs does not vary in-between solutions.

To validate these etching procedures, we also prepared quantum rods with thinner shells by varying the temperature (two monolayers (DR-2) and one monolayer (DR-3), Figure 1, Figure 2, Table 1). To compare with results reported in the literature,[10, 28] we used the same ligands exchange process to directly modify DRs with cysteine without the benzylamine treatment process. These CdSe/CdS DRs were also transferred to a water solution containing the L- or D- cysteine solution (2 mL), and the reaction mixture was deoxygenated and stirred at room temperature under argon in the dark for 24 h to obtain the chiral DRs.

A comparison of the chiral signals of these different DRs is shown in Figure 6, Figure S5, Table 4 for the 500-650 nm range, and Figure 7, Figure S6, Table 5, for the 350-500 nm range; they are consistent with the etching results (Figure S2 and Figure S3). The chiral signal of the CdSe cores increases when the shell thickness decreases (Figure 6, Figure S5, and Table 4), as reported in the literature,[17] indicating that the smaller the distance between the ligand and the core, the stronger the chiral signal.

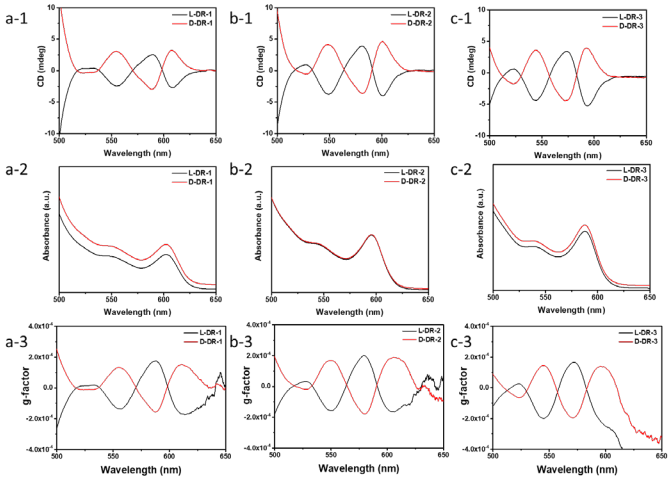

Figure 5. The corresponding CD, UV-vis., and g-factor variations of DRs with different shell thicknesses at the first exciton absorption peak. a) Three-monolayer DR-1 after Cys exchange, b) two-monolayer DR-2 after Cys exchange, c) one-monolayer DR-3 after Cys exchange.

Table 4. CD and g-factor of L-Cys-DRs with different shell-thicknesses at the first exciton absorption peak.

	UV-vis. (nm) (core)	CD^+/λ_{CD}[a]	CD^-/λ_{CD}[b]	$\lvert CD^+ - CD^- \rvert/2$[c]	g_{CD+}/λ_{CD}[d]	g_{CD-}/λ_{CD}[e]	$\lvert g_{CD+} - g_{CD-} \rvert/2$[f]
DR-1	602.4	2.539/ 589.2	-2.691/ 609.4	2.615	1.748/ 588.0	-1.717/ 613.0	1.733
DR-2	595.8	3.907/5 81.2	-4.002/ 600.8	3.955	1.972/ 578.2	-1.629/ 605.1	1.801
DR-3	587.8	3.410/5 74.2	-5.252/ 593.6	4.331	1.650/ 572.3	-2.324/ 596.9	1.987

[a, b] CD anisotropy at the most intense positive and negative CD bands (mdeg/nm), [c] magnitude of the CD signal, defined as $\lvert CD^+ - CD^- \rvert/2$, [d, e] CD anisotropy g_{CD}-factors at the most intense positive and negative CD bands (10^{-4}/nm), [f] magnitude of the g_{CD} factor ($\lvert g_{CD+} - g_{CD-} \rvert/2$) ($10^{-4}$/nm). DRs were treated without benzylamine ligand exchange.

Please do not adjust margins

Please do not adjust margins

Table 5. The CD and g-factor of L-Cys-DRs with different shell-thicknesses (350-500 nm).

Name	UV-vis. (nm)	CD^+/ λ_{CD}[a]	CD^-/ λ_{CD}[b]	$\lvert CD^+ - CD^- \rvert/2$[c]	g_{CD+}/ λ_{CD}[d]	g_{CD-}/ λ_{CD}[e]	$\lvert g_{CD+} - g_{CD-} \rvert/2$[f]
DR-1	602.4	13.772/ 468.4	-27.786/ 482.3	20.779	1.733/ 468.7	-6.092/ 485.0	3.913
DR-2	595.8	35.315/ 462.8	-45.223/ 477.0	40.269	4.317/ 462.7	-9.776/ 480.6	7.047
DR-3	587.8	23.027/ 454.3	-24.913/ 469.6	23.970	4.905/ 454.1	-8.793/ 472.6	6.849

[a, b] CD anisotropy at the most intense positive and negative CD bands (mdeg/nm), [c] magnitude of the CD signal, defined as $|CD^+ - CD^-|/2$, [d, e] CD anisotropy g_{CD}-factors at the most intense positive and negative CD bands (10^{-4}/nm), [f] magnitude of the g_{CD} factor, defined as $|g_{CD+} - g_{CD-}|/2$. DRs were treated without benzylamine ligand exchange.

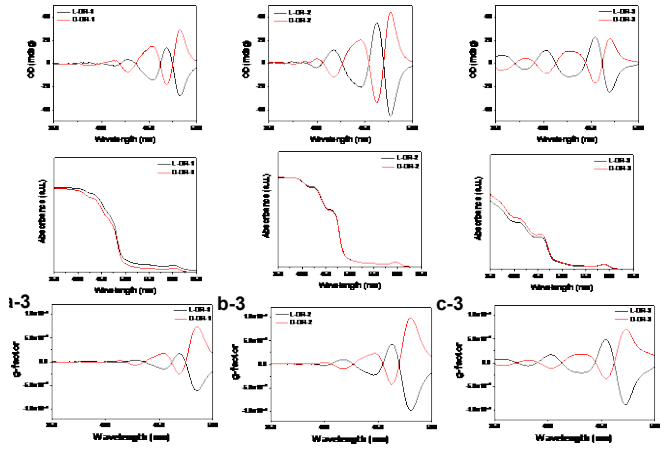

Figure 6. The corresponding CD, UV-vis., and g-factor variations of DRs with different shell thicknesses (350-500 nm). a) Three-monolayer DR-1 after Cys exchange. b) Two-monolayer DR-2 after Cys exchange, c) One-monolayer DR-3 after Cys exchange. The concentration is 5 times lower than in Figure 6.

However, due to the poor control of the one-pot bottom-up method, it is difficult to prepare samples controlling only one variable (the shell-thickness or length), indeed here despite our attempts both of them varied from one experiment to the other (see Table 1) and this influences the global chiral reply. Then, as illustrated in Figure 7, Figure S6, and Table 5, different from what is observed in the etching process which shows the true evolution, the chiral signal of the CdS shell (below 500 nm) in bulk solution is also complex and depends on the thickness, this further prevents the chiral study of individual particles justifying this work.

Use of thinner shell

To push the system and further improve the chiral signal, we tried to etch the thinnest shell of the DR-3 sample. It was expected that through further etching, the CdS protection would be removed and the CdSe core would be completely exposed and directly in contact with the chiral ligands, minimizing the distance between the ligands and the CdSe core, thereby further improving the chiral conduction effect and enhancing the chiral signal.[17, 25] Surprisingly, as shown in Figure 8, Figure S7, Figure S8, and Table S2, the experimental results were opposite to the expectations. Indeed, as the etching proceeded from 1 to 4 cycles, the CD signal at the first exciton absorption peak did not increase as expected but decreased (Figure 8), while the corresponding UV-vis. absorption peak underwent a blue shift (Figure S7f), due to the core etching (see below). Additionally, the corresponding g-factor still showed a different evolutionary process than the CD signal, since it first increased and then decreased (Figure S7 and Figure S8), showing once more, that simply using the g-factor to accurately represent the change in chiral signal behaviour of a single nanoparticle was not the best solution.

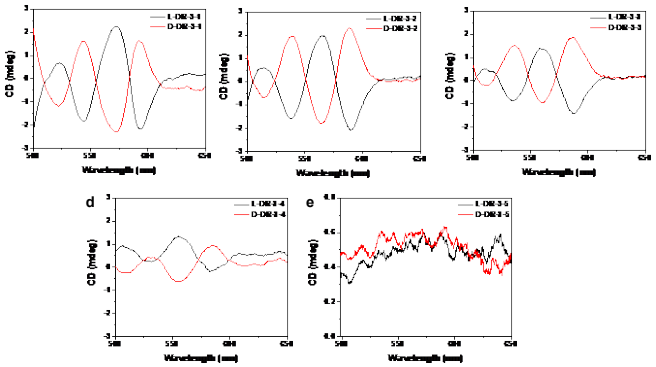

Figure 7. CD spectra variations of DR-3 at the first exciton absorption peak during the etching process. (a) CD spectra of benzylamine-modified DRs after Cys exchange; (b)-(e) CD spectra of DRs one cycle to four etching cycles after Cys exchange.

From all these results, we then conclude that one monolayer is in fact the best compromise to get the highest values for both g-factor and CD because below, a chemical etching of the core takes place and necessarily induces a decrease of the chiral signal.

To explore the behaviour of this abnormal change in chirality, we conducted an in-depth study on the one-monolayer shell sample (DR-3) by TEM and XRD analyses (Figure 9). First, as the etching process proceeds, obvious defects appear at the position of the CdSe core (the core is consumed, as shown by the curvature in the DRs (red outlines in Figure 9b-d), while broken nanorods appear as the etching further goes on (Figure 9d-e, orange ellipses).

The X-ray diffraction (XRD) patterns and corresponding diffraction peaks of the synthesized CdSe/CdS DRs (DR-3-1) match well with the crystalline structure of w-CdS (JCPDF No. 41-1049) (Figure 9f (black)).[56] While, as the etching progresses (Figure 9f (red and blue)), the crystal shape of the etched samples (DR-3-2 and DR-3-4) gets degraded and the signal gradually decreases. This is consistent with the literature where Brock's and Peng's groups reported that peroxides can etch CdSe much more efficiently than CdS.[46, 57] In fact, in the thick-shell samples (DR-1), isotropic etching of the CdS shell is observed. Only a well-protected CdSe core nanocrystal can be used for the isotropic etching of the shell, and any pinhole in the CdS shell allows etching of the inner CdSe core since Se is more easily oxidized than S.[44, 46] In the thinnest shell case, with etching at some point the CdS shell can no longer fully protect the CdSe core with a thickness of less than one layer; then, this preferential etching of the CdSe core leads to the observed anisotropic etching.[45] This is the main reason for the reduction

Please do not adjust margins

in the CD signals of these thin-shell CdSe/CdS DRs after etching (Figure S7 and Figure S8).

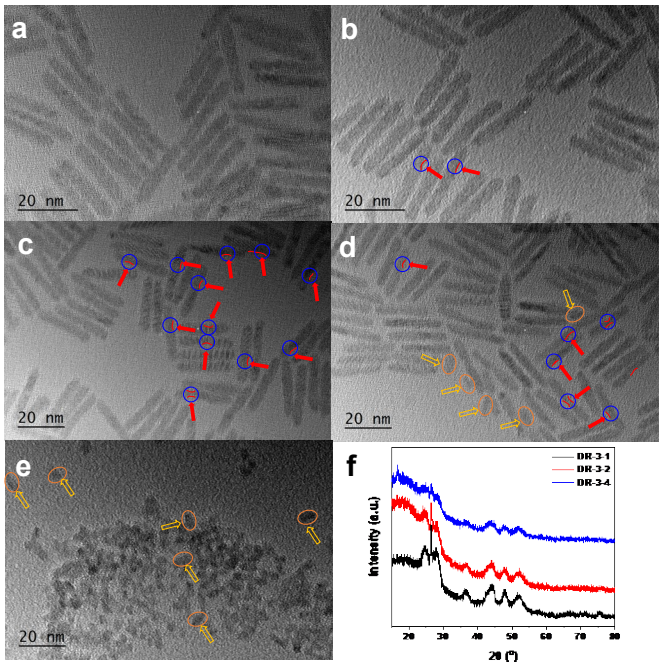

Figure 8. TEM images and XRD pattern of DR-3 after the etching process. a) TEM of benzylamine modified DRs; b)-e) TEM of DRs after one cycle to four etching cycles. The red outline represents the etched part, the blue circles show the CdSe core position, and the orange ones, quantum rods that have been etched and broken. f) Corresponding XRD patterns of DR-3 after etching processes (a, b, and d).

This core etching affects the transfer of electron holes between the core and the shell, thereby reducing the ligand-induced chiral transfer in this domain of wavelengths (< 500 nm). TEM images (Figure 9, S9(for the original image), also show that in the case of the thin-shell DR-3, the preferential etching of the CdSe core (Figure 9b-d), eventually leads to nanorod break-down (Figure 9d-e). This means that 1ML thin-shell CdSe/CdS DRs cannot be used in the top-down chemical etching process for a further improvement of chirality as proposed, because they are probably already in their best configuration with a good compromise between high chiral signals and appropriate CPL properties.

Additionally, based on the etched position, we can infer the position of the CdSe core (Figure 9 b-d, blue circles): most of the DRs cores are located at 1/4 to 1/2 of one of the tips, which is consistent with the literature.[58-60] This top-down chemical etching technology can then also be used to characterize the position of the core in DRs, in a much cheaper way than the expensive HAADF-STEM generally reported in the literature for such determination.[58, 60]

Comparison of the chiral signals in the thick and thin shell DRs

This difference in behaviour can also be verified by monitoring the changes in the UV-vis. absorption spectra of these two types of DRs. Due to the different etching speeds of the CdS shell and CdSe core, samples with different shell thicknesses (DR-1, DR-3) do show different trends under the same etching process. In the thin-shell DR-3, the anisotropic etching process induces a significant blue shift of the emission wavelength, and at the same time, the CdSe first exciton peak sharply decreases or even disappears (orange spectrum) (Figure S7f). Meanwhile, in the thick-shell DRs (DR-1, Figure S2d), thanks to the better protection of the CdSe core, the absorption spectrum gradually shifts to higher energy (blue spectrum) by only 2 nm under the isotropic etching and maintains the contour and the peak width of the UV-vis. spectrum of the original DRs (the absorption remaining constant as expected).

Figure 10 plots the dependence of the DR-1 and DR-3 absorbance on the etching time for two wavelengths (450 nm and the first exciton absorption peak).

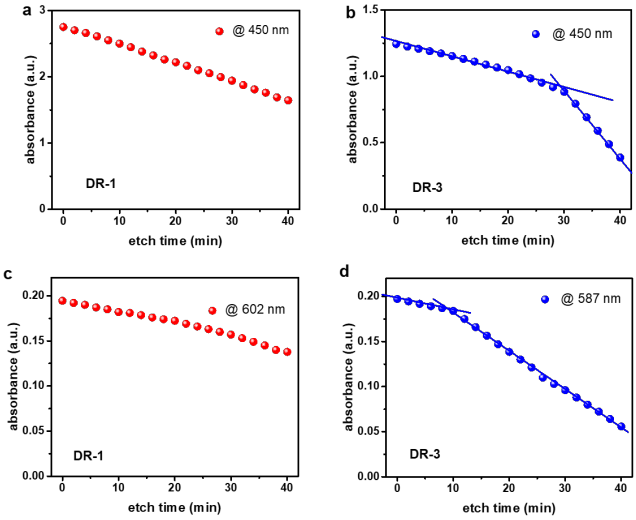

Figure 9. The dependence of the absorbance on the etching time at two wavelengths (450 nm and the first exciton absorption peak) for DR-1 and DR-3. a), c) DR-1 with thick CdS shell (3ML); b), d) DR-3 with thin CdS shell (1ML). The DRs samples were tested in 5 times diluted solutions. These data indicate that the etching process for the thin shell DR3 has two stages.

In the case of the thin shell DR-3, the change in the slope of these dependencies clearly indicates the transition between two different etching stages for either wavelength. The initial slow change in absorbance is associated with the removal of the CdS shell (1.12×10^{-2} units/min at 450 nm and 1.3×10^{-3} units/min at 602 nm), while the second one significant of faster changes is due to a quicker dissolution of the CdSe core, because (i) Se is more easily oxidized and (ii) any pinhole in the CdS protective shell is detrimental for the core (5×10^{-2} units/min at 450 nm and 4×10^{-3} units/min at 587 nm).[45] Meanwhile, for the thick shell DR-1, the etching time linearly varies with time for DR-1 with one main shell etching process taking place. This etching of the CdSe core generates numerous defects which affect the electron-hole transport between the core and the shell, prevent ligand-induced chiral conduction, and significantly reduce CD signals (Figures 8 and S8). Another item to note is the g-factor behaviour that first increases and then decreases, with the CdSe core etching which decreases the absorption of the first exciton absorption peak at a given concentration (Figure S7f) and the CD signal. Then, in such a situation, even if both the CD and UV-vis. signals decrease, the calculated g-factor at the first exciton absorption peak may still increase within a given range (Figure S7), for both the CD and UV-vis. curves have different slopes

Please do not adjust margins

(Figure S8) and intercross. This result can be very confusing when considering only one aspect of the growth process. If a study is based only on the g-factor, it may lead to a different and probably misleading approach to the mechanism of action.

Although it is impossible to further enhance the chiral signal of the thin-shell DRs (< 1ML) by etching, we can still analyze the reason for this DR high chiral signal through the etching process looking at the chiral signal of the CdS shell. It has been mentioned in the literature that in DR nanoparticles, the chiral signal of the CdS shell was often found to be much larger than that of the core.[10, 28, 35] Kuang *et al.* showed for example that based on a two amino acid post-synthetic ligand exchange strategy, long CdSe/CdS semiconductor nanorods could induce strong chirality properties with g-factors even higher than 10^{-3} (1.2×10^{-3}/461 nm),[35] which had great potential for chiral applications of the CdS shell.

Then, considering our results above, we can assume here that the concentration of DRs in solution is constant and no changes should be observed in the controlled etching experiments, by monitoring the absorption before and after the ligand exchange process. As a consequence, the CD intensities in Figure 11, then directly reflect the chiral properties of a given concentration of DRs under an etching process; thus, that of a single nanoparticle.

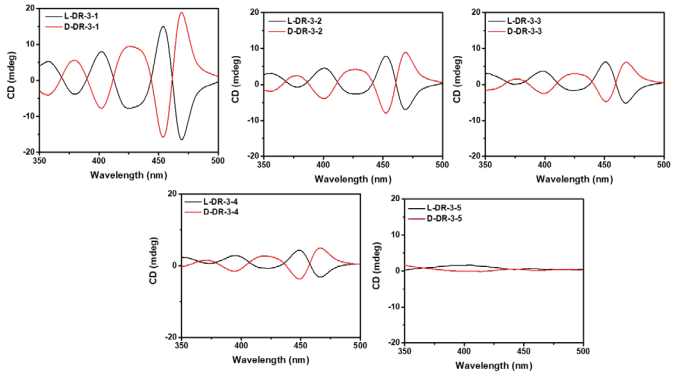

Figure 10. Variation of the CD spectrum of DR-3 during the etching process (< 500 nm). (a) CD spectrum of benzyl amine-modified DRs after Cys exchange; (b)-(e) CD spectrum of DRs one cycle to four etching cycles and after Cys exchange. The concentration is 5 times lower than that in Figure 8.

Comparing Figure S4 and Figure 12, it looks obvious that the CD chiral signal of the CdS shell (< 500 nm) of the individual nanoparticle follows the same behaviour, a decrease with etching and this regardless of the initial shell thickness. In the case of the thin shell sample (DR-3) (Figure 12), besides the surface decrease of the CdS shell, and thereby a decrease of the amount of adsorbed chiral ligands on the surface, as a first reason, the etching of the CdSe core should also be considered. This is confirmed by the dependence of the absorbance on the etching time for DR-3 in Figures 10b and d, which shows these two stages: a slow decrease in the first stage followed by an abrupt break in slope[45, 61] in the second stage. The CdSe core etching will further affect the electron and hole transport between the core and the shell, thereby preventing the CD signal of the shell.

Moreover, after the most severe etching (Figure 13 e), the DRs show a signal of the same order (10^{-5}) as that of the CdS quantum dots.[20] At this point, the CdSe core is completely etched, and the chiral transmission between CdS and the ligands is the only process that can take place. Through the study of the etching experiment, we can see that the CdSe core is also a key factor in the process of generating high chiral signals in DRs.

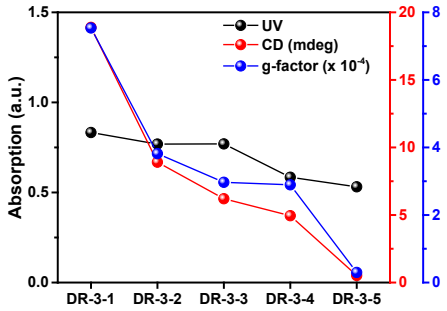

Figure 11. The CD, UV-vis., and g-factor variations of L-Cys-DR-3-n (n = 1-5) during the etching process (< 500 nm). DR-3-1: benzyl amine-modified DRs after Cys exchange; DR-3-2 to 5: one to four etching cycles and after Cys exchange. The UV-vis. value is the maximum value of the CD signal. The concentration is 5 times lower than that in Figure S7.

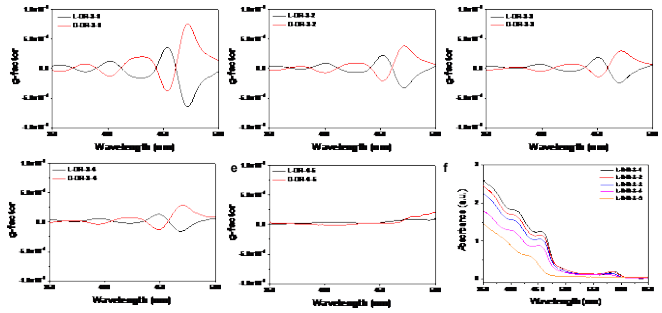

Figure 12. The corresponding UV-vis., and g-factor variations of DR-3 as shown in Figure 11 (< 500 nm). a) CD spectrum of benzyl amine-modified DRs after Cys exchange, b-e) the CD spectrum of DRs after one to four etching cycles and Cys exchange, f) corresponding UV-vis. absorption of different etching processes. The concentration is 5 times lower than in Figure S7.

This may also be the reason why compared to CdSe or CdS NCs (dots or even rods)[5, 20], the CdSe/CdS DRs exhibit much higher CD signals[10, 35], especially in the sub-500 nm range for the CdS shell region. Whereas, when directly using the g-factor for comparison, the results can be complicated and misinterpreted (Figure 5, Figure S4 and Figure 12, Figure 13). We can conclude that comparative experiments in between series, cannot be performed with confidence since the molar absorption coefficient of a single nanoparticle often changes greatly especially in the range below 500 nm, which affects the number of nanoparticles per mole for a given absorbance value. In this case, the g-factor exhibits chiral signals for different numbers of nanoparticles per mole, which does not provide the real chiral signal of a single nanoparticle. The same problem arises in the etching process to study chirality by g-factor, which causes g-factor to be seriously affected by the change in the molar absorption coefficient of a single nanoparticle and then hides the true chiral change law.

Role of the core size

Thin shell DRs (DR-4 and DR-5) with different CdSe core sizes (Table 1) were also used for comparison and generalization, and the same pattern was found, i.e., a CD chiral signal increase with both the shell (DR-1, DR-2, and DR-3) and the core size ((DR-5, DR-4, and DR-3) decrease. Furthermore, as soon as the CdSe core is exposed, it is preferentially etched, thereby weakening the chiral signal of the first exciton peak (CdSe core) of the single nanoparticle (Figures S10 and S11). This increases the defects on the surface of the CdSe core, which disrupts its interaction with the chiral ligands, resulting in a sharp decrease in the CD signal.

For the DRs with cores of different sizes (DR-3 to DR-5 in Table 1), the chiral signal decrease in the CdS shell range (< 500nm) with the core increase (Figure 14) is spectacular. This may be because DRs with a larger core size, are of type I structure[62] which implies that the confinement of the electron is in the shell rather than in the core, while, DRs with a small CdSe core are closer to a quasi-type II,[63] which makes the electrons easily delocalized, thereby enhancing the transmission of chiral signals.

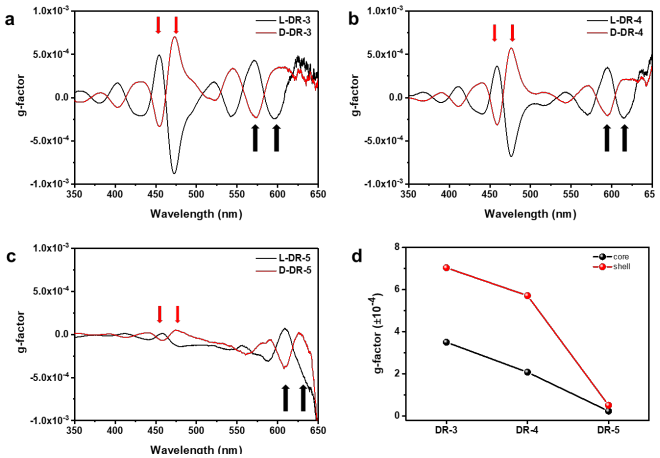

Figure 13. The g-factor variation of DRs with different core sizes. a) DR-3, b) DR-4, c) DR-5, d) the g-factor value variation for the position of core and shell (The peaks are marked by a black or red arrow, respectively).

CPL study of the thin-shell DRs.

The development of circularly polarized luminescent (CPL) materials has drawn extensive attention due to their numerous potential applications in optical data storage, displays, backlights in 3D displays, and so on. In developing CPL materials, the key issue is to obtain a high luminescence dissymmetry factor (g_{lum}), which is used to quantify the level of CPL.

We studied the change in the CPL signal of the DRs with etching, as illustrated in Figures S12 and S13. In the case of the thin shell DR-3, the CPL signal gradually decreases with the etching. Coupling these data with our previous work,[28] which shows the opposite, i.e., that the CPL signal gradually decreases with the shell thickness increase, we can confirm here also with CPL that DRs with a limit of 1ML is the best configuration for the highest chiral properties.

The mechanism

Based on the different oxidative activities of the two chalcogenides,[45] and these results, we propose the following mechanism (Scheme 1). The etching of CdSe/CdS DRs is divided into two steps: First, the CdS shell is slowly etched, and the CD chirality of CdSe increases with the shell CdS thickness decrease. It goes through a maximum value corresponding to about one monolayer of CdS (1ML). In the second stage, CdSe is quickly etched due to its exposure, and the chirality induced by the CdSe core significantly decreases. The CD signal of the CdS shell in these solutions of identical DRs concentration does decrease in both stages, and the g-factor variation shows that the overall reactions are complex and should not be considered on their own to perform comparison in between samples.

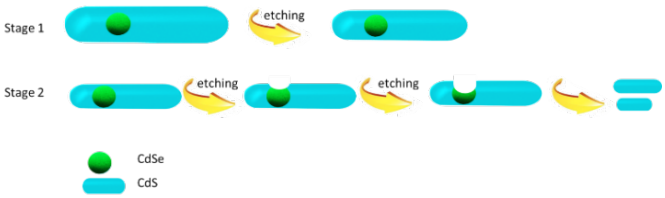

Scheme 1. The schematic diagram of the DRs etching process.

With the above analysis, one would picture that the controlled etching process proceeds via an outer surface mechanism in a layer-by-layer procedure, which gradually removes the Cd and S atoms from the surface. Once the CdS shell around the CdSe core is thin enough (stage-2), both CdSe and CdS are etched simultaneously, causing a sharp decrease in chirality and absorbance. During the first stage, the absorption below 500 nm decreases slowly (Figure 10b), and the first exciton absorption peak blue-shifts a little (Figure S2d), accordingly.[64] Consistent with the matched absorption spectra, the TEM images of the etched DRs show practically the same size distribution as the original CdSe/CdS nanocrystals (Figure 9a-b), within the experimental errors.

During the second stage, the etching rate becomes significantly faster as indicated by the quick changes of the first exciton absorption peaks in the absorption spectra (Figure 10d) and the TEM images of the etched DRs which exhibit worse size distributions (Figure 9d-e). Indeed, when BPO reaches the more reactive CdSe surface, the etching rate speeds up as observed experimentally (Figure S7f, Figure 10d), [46, 61] sulfides being much more difficult to oxidize than selenides, leading to rapid oxidation and even dissolution of the CdSe cores and the generation of a population of smaller CdS quantum rods. This explanation is consistent with the disappearance of the first exciton absorption peak of the CdSe core in the absorption spectra.

Please do not adjust margins

In fact, the overall mechanism is not yet fully understood even if some insights have recently begun to appear in the literature.[14, 65] It is assumed that the induced chiroptical activity that is observed in QDs and DRs originates from hybridization of the highest occupied molecular orbital (HOMO) level of cysteine and the valence band (VB) level of the DRs, resulting in a decrease of the energy bandgap and a concomitant redshift of the CD and fluorescence spectra relative to the bare DRs.

What is also certain is that using CdSe as a core and its interaction with the CdS shell in a rod rather than a simple rod-like CdS structure, significantly enhances the chiral signal. Basically, when the core is coated by a shell of another semiconductor with a wider bandgap, a conduction band higher in energy and a valence band lower in energy than the core, form a structure with the effect of confining the excited state to the nanoparticle core. When the shell is corroded enough to observe the core etching, more defects form and the nanorods eventually break, resulting in a sharp decrease in the chiral signal. In other words, this may indirectly explain that the coexistence of the core and a one-monolayer shell of two different natures is crucial for a high chiral signal.

Our research work has shown that:

by studying the chirality changes in nanoparticles in solutions of identical concentration, it becomes possible to compare more accurately, which may guide the achievement of the exploration of signals with higher chirality.

using the g-factor alone and ignoring the CD signal to avoid the influence of the concentration and the oscillator strength when comparing different samples can lead to erroneous interpretations.

Experimental

Chemicals*:* Tri-n-octyl phosphine oxide (TOPO, 99%), tri-n-octyl phosphine (TOP, 97%), tributyl phosphine (TBP, 99%), n-octadecyl phosphonic acid (ODPA, 97%), and n-hexyl phosphonic acid (HPA, 97%) were purchased from Strem Chemicals. Cadmium oxide (CdO, 99.99%), selenium (Se, 99.99%), sulfur (S, 99.98%), Benzyl amine (99%), and tetramethylammonium hydroxide pentahydrate (TMAH, 97%) were purchased from Sigma-Aldrich. Benzoyl peroxide (BPO, AR), L-cysteine hydrochloride monohydrate (L-Cys, 99%), and D-cysteine hydrochloride monohydrate (D-Cys, 99%) were purchased from Aladdin Industrial Co., Ltd. (Shanghai, China). Pure water was purchased from Hangzhou Wahaha Group Co., Ltd, China. All chemicals were used as received without further purification.

Characterization*:* Transmission electron microscopy (TEM) experiments were carried out with a JEOL JEM1400 Plus microscope operating at 120 kV, and an FEI Tecnai G2 F30 operating at 300 kV. To be representative and statistically meaningful, many images from several regions of various samples were recorded and the most characteristic results are presented here, and at least 200-250 NPs were treated. T The UV/vis. absorption measurements were performed using a TU-1901 double-beam UV/vis. spectrophotometer (Beijing Purkinje General Instrument Co. Ltd., China), and the photoluminescence (PL) spectra were recorded on a fluoroSENS spectrophotometer (Gilden Photonics). The absolute PL quantum yields (QYs) of the QDs solutions were measured using an Ocean Optics FOIS-1 integrating sphere coupled with a QE65 Pro spectrometer.[66, 67]

CD measurements: The measurements were conducted on a JASCO J-1500 CD spectrometer at a scan rate of 20 nm/min. All CD experiments were carried out in Milli-Q water with a quartz cuvette (0.1 cm path length, Hellma). In designing chiral nanoparticles for application, the anisotropy or g-factor is a key parameter to determine the optical activity due to its ready availability by comparing the CD spectrum with the absorption spectrum. The equation is as follows: $g = \theta/(3.298 \times 10^4 \times A)$, where ɵ is the vertical coordinate of CD spectrum, and A is the value in the absorption spectrum at the concentration used to measure the CD spectrum.

CPL measurements*:* The CPL measurements were performed on a JASCO CPL-300 spectrometer in Milli-Q water with a quartz cuvette (0.1 cm path length, Hellma) with an excitation wavelength of 400 nm.

All the optical measurements were performed at room temperature under ambient conditions.

Synthesis of spherical CdSe core. The synthetic procedure was based on the procedure reported in the literature.[52, 53, 63, 68, 69] Typically, TOPO (1.5 g), ODPA (0.140 g), and CdO (0.030 g) were mixed in a 50 mL flask, heated to 150 °C and alternately exposed to vacuum and argon at least 5 times until CdO was a brown solid and the rest of the reagents were a colourless liquid. Then, to dissolve the CdO, the solution was heated to above 320 °C under argon until it became optically clear and colourless, which indicated that the reaction between CdO and ODPA was complete. Then, the temperature was increased to 350 °C, and 1.5 mL of TOP was injected into the flask, which caused the temperature to naturally decrease to 300 °C. A tri octyl phosphine selenide (Se-TOP) stock solution of concentration 1.0 M selenium in TOP was prepared by addition of selenium powder (1184.4 mg, 15 mmol) to a 20 mL vials with a stir bar. The vial was filled with argon (Ar) and then, 15 mL of TOP (97%) was added to the vial via syringe, and the resulting mixture was sonicated, stirred, and vortex mixed until homogeneous. This Se:TOP solution (0.4 mL, 1 mol/L) was then injected at 380 °C and reacted for several seconds. The size of the CdSe core was adjusted by controlling the temperature and reaction time.

The CdSe core solution was then purified according to the following procedure. It was maintained to 70~80 °C, and 4 mL of ethanol and a certain amount of TBP were added into the above solution, which was centrifuged at 10000 rpm for 3 minutes. Then, the precipitate was dissolved in a small amount of toluene while the supernatant was discarded. After centrifugation again, the precipitate was dissolved in TOP (CdSe-TOP). Due to the TBP purified process, the CdSe core can be better purified, which can remove the adsorbed ions on the surface and the by-products in the solution. This is essential for uniform morphology control and high quantum yield.

The amount of CdSe seeds was determined with absorption spectroscopy using the empirical formulas of Peng et al.[37] which

correlates the position of the first electronic transition with the diameter of the CdSe particles (equation 1) and the molar extinction coefficient of the particles and their diameter (equation 2).

$$D = 1.6122 \times 10^{-9} \cdot \lambda^4 - 2.6575 \times 10^{-6} \cdot \lambda^3 + 1.6242 \times 10^{-3} \cdot \lambda^2 - 0.4277 \cdot \lambda + 41.57 \quad (1)$$

$$\varepsilon = 5857 \cdot (D)^{2.65} \quad (2)$$

Synthesis of CdSe/CdS DRs.[10] In a typical synthesis of CdSe/CdS dot-in-rods (DRs) via seeded growth, CdO (180 mg) was mixed in a 100 mL flask together with TOPO (6 g), ODPA (600 mg), and HPA (180 mg). Concomitantly, a tri-n-octyl phosphine sulfur (S-TOP) stock solution of concentration 2.5 M sulfur in TOP was prepared by addition of sulfur powder (1200 mg, 37.5 mmol) to a 20 mL vials with a stir bar. The vial was filled with Ar and then, 15 mL of TOP (97%) was added to the vial via syringe and heated at 120 ˚C, the resulting mixture was sonicated, stirred, and vortex mixed until homogeneous. After alternately exposing the CdO containing flask to vacuum and argon at least 5 times at 150 °C, the resulting solution was heated to 300 °C to make the solution become a completely transparent liquid without any solids. 3.0 mL of TOP was added, and then, the temperature was increased to 320 °C and a mixed solution of S:TOP (3.0 mL, 2.5 mol/L) and the above CdSe-TOP solution (600 µL) were injected into the flask, which caused the temperature to naturally dropped to 270~300 °C and then recovered to the pre-injection temperature within two minutes. The CdSe/CdS DRs were allowed to grow for approximately 8 minutes after the injection. Finally, the reaction mixture was cooled to room temperature, and an extraction procedure was used to separate the nanocrystals from the side products and unreacted precursors.

General procedure for shell thickness and aspect ratio control. The CdSe/CdS DRs with different shell thicknesses can be synthesized under different injection temperatures. For instance, using the CdSe with a 578 nm PL emission as a core, by changing the injection temperature from 320 to 380 °C, the shell thickness changed from 0.35 nm to 1.05 nm.

Controlled Etching. Controlled etching of nanocrystals with benzoyl peroxide (BPO) was performed following the technique described in the references.[43, 44, 46]

Before etching of CdSe/CdS DRs with BPO, their surface ligands were exchanged with a shorter benzylamine by mixing respectively 2 mL of purified CdSe/CdS DRs in chloroform with 5 mL of benzylamine, and the resulting suspension was sonicated for 20 min until the solution turned clear. For the further etching process, 36 mL of a toluene/methanol (3:1) mixture was added to the DRs mixture solution, and then 0.3 mL of BPO solution (0.2M) were further injected into the nanocrystals suspension and allowed to react for 10 min, after which the absorbance was measured. This step was repeated several times for the following-up study about the mechanism of chiral conduction of Cys-DRs. Etched NCs were precipitated with ethanol and re-dispersed in chloroform.

For the test of UV-vis. absorbance on the etching time, we take one measurement every two minutes to get the evolution of absorbance.

Ligand Exchange on the CdSe/CdS DRs with Chiral Cysteine Molecules.[10, 12, 14] D- or L-cysteine hydrochloride monohydrate (0.2 M) was dissolved in DI water, and then the pH of the solution was adjusted to 12 by TMAH to form the cysteine solution. Then, a solution of CdSe/CdS DRs with or without etching in chloroform (2 mL) was added to the cysteine solution (2 mL), and the reaction mixture was deoxygenated and stirred at room temperature under argon in the absence of light for 24 h. The reaction mixture was left to stand for 1 h to allow the phases to separate. The top aqueous layer was got with a syringe, and the Cys-CdSe/CdS DRs were purified by precipitation with ethanol/DI water (4:1, 2 times). The purified Cys-DRs were dissolved in DI H_2O and stored at room temperature in the dark.

For the normal ligand exchange process, such as the comparison of DR-1, DR-2 and DR-3, the ligands of DRs were directly exchanged by Cys without the step with benzylamine and BPO etching treatment process. Which is the same process as the reference.[10, 28]

Conclusion

In conclusion, we have proposed a method to verify the evolution of ligand-induced chiral conduction mechanism using a *top-down* etching process, which can in principle be applied to any type of complex nanocrystals, especially core-shell structure materials. This technique complements the traditional approach to the chiral conduction mechanism by providing a series of homologous nanocrystals that cannot be easily obtained using bottom-up colloidal synthesis methods. In the present study, a facile top-down etching procedure was employed to fabricate CdSe/CdS DRs where both the CdSe core and CdS shell components were etched in a controlled step-by-step process. Once the outer layer CdS was etched away, the core was gradually exposed on the side of the rod and preferentially etched at this location in the second stage due to the much higher reactivity of selenide compared to sulfide. This top-down approach results in a series of solutions of identical concentrations of DRs with various shell thicknesses. It provides an opportunity that the bottom-up approach is not able to do at this stage since a reaction per number of layers and temperature has to be launched independently.

Then, this etching approach allows the comparison of solutions of NPs at the same concentration. As long as the core is not etched, the comparison of such solutions of NPs shows that the chiral signal of the CdSe core gradually decreases with the shell-thickness increase, while the chiral signal of the shell layer increases. Through a series of comparative studies of chiral signals induced by solutions of NPs at the same concentration, the results show that the chiral signal comparison of a single nanoparticle can be better used to study the chiral change rules compared to the g-factor in a bulk system.

The CD and CPL activities could be further modulated via top-down chemical etching, and the origin of highly induced chirality for DRs was elucidated to mainly involve the dot-in-rod

Please do not adjust margins

Please do not adjust margins

structure, especially the interaction between the core and the shell. To our knowledge, the present work is the first demonstration of the mechanism of ligand-induced chiral transmission through a top-down etching process. We expect this etching-after-growth approach will find versatile applications in the future to design widespread applications in different chiral mechanism research systems with the highest precision

Author Contributions

The manuscript was written through the contributions of all authors. All authors have approved the final version of the manuscript.

‡These authors contributed equally.

Conflicts of interest

There are no conflicts to declare.

Acknowledgments

MHD acknowledge the CNRS through the MITI interdisciplinary programs (Action MITI: Nouveaux Matériaux 2020 and 2021). This work was supported by the funding support from the Ministry of Science and Technology of China (Nos. 2016YFB0401702 and 2017YFE0120400), National Natural Science Foundation of China (Nos. 61875082, 61405089, and 62005115), Key-Area Research and Development Program of Guangdong Province (Nos. 2019B010925001, and 2019B010924001), Shenzhen Key Laboratory for Advanced Quantum Dot Displays and Lighting (No. ZDSYS201707281632549). TEM data were obtained using equipment maintained by the Southern University of Science and Technology Core Research Facilities, and the authors acknowledge the technical support from Dongsheng He and Yang Qiu in SUSTech CRF.

References

1. E. Shah and H. P. Soni, Inducing chirality on ZnS nanoparticles for asymmetric aldol condensation reactions, *RSC Advances*, 2013, **3**, 17453-17461.
2. Y. Xia, Y. Zhou and Z. Tang, Chiral Inorganic Nanoparticles: Origin, Optical Properties and Bioapplications, *Nanoscale*, 2011, **3**, 1374-1382.
3. M. Sun, L. Xu, A. Qu, P. Zhao, T. Hao, W. Ma, C. Hao, X. Wen, F. M. Colombari, A. F. de Moura, N. A. Kotov, C. Xu and H. Kuang, Site-selective photoinduced cleavage and profiling of DNA by chiral semiconductor nanoparticles, *Nature Chemistry*, 2018, **10**, 821-830.
4. A. Kühnle, T. R. Linderoth, B. Hammer and F. Besenbacher, Chiral recognition in dimerization of adsorbed cysteine observed by scanning tunnelling microscopy, *Nature*, 2002, **415**, 891-893.
5. A. Ben-Moshe, A. Teitelboim, D. Oron and G. Markovich, Probing the Interaction of Quantum Dots with Chiral Capping Molecules Using Circular Dichroism Spectroscopy, *Nano Letters*, 2016, **16**, 7467-7473.
6. S. V. Lobanov, T. Weiss, N. A. Gippius, S. G. Tikhodeev, V. D. Kulakovskii, K. Konishi and M. J. O. l. Kuwata-Gonokami, Polarization control of quantum dot emission by chiral photonic crystal slabs, *Optics Letters*, 2015, **40**, 1528-1531.
7. K. Konishi, M. Nomura, N. Kumagai, S. Iwamoto, Y. Arakawa and M. Kuwata-Gonokami, Circularly Polarized Light Emission from Semiconductor Planar Chiral Nanostructures, *Physical Review Letters*, 2011, **106**, 057402.
8. Y. Zhou, M. Yang, K. Sun, Z. Tang and N. A. Kotov, Similar Topological Origin of Chiral Centers in Organic and Nanoscale Inorganic Structures: Effect of Stabilizer Chirality on Optical Isomerism and Growth of CdTe Nanocrystals, *Journal of the American Chemical Society*, 2010, **132**, 6006-6013.
9. M. V. Mukhina, V. G. Maslov, A. V. Baranov, A. V. Fedorov, A. O. Orlova, F. Purcell-Milton, J. Govan and Y. K. Gun'ko, Intrinsic Chirality of CdSe/ZnS Quantum Dots and Quantum Rods, *Nano Letters*, 2015, **15**, 2844-2851.
10. J. Cheng, J. Hao, H. Liu, J. Li, J. Li, X. Zhu, X. Lin, K. Wang and T. He, Optically Active CdSe-Dot/CdS-Rod Nanocrystals with Induced Chirality and Circularly Polarized Luminescence, *ACS Nano*, 2018, **12**, 5341-5350.
11. J. Yeom, B. Yeom, H. Chan, K. W. Smith, S. Dominguez-Medina, Joong H. Bahng, G. Zhao, W.-S. Chang, S.-J. Chang, A. Chuvilin, D. Melnikau, A. L. Rogach, P. Zhang, S. Link, P. Král and N. A. Kotov, Chiral Templating of Self-Assembling Nanostructures by Circularly Polarized Light, *Nature Materials*, 2014, **14**, 66.
12. U. Tohgha, K. K. Deol, A. G. Porter, S. G. Bartko, J. K. Choi, B. M. Leonard, K. Varga, J. Kubelka, G. Muller and M. Balaz, Ligand Induced Circular Dichroism and Circularly Polarized Luminescence in CdSe Quantum Dots, *ACS Nano*, 2013, **7**, 11094-11102.
13. Y. Shi, Z. Zhou, X. Miao, Y. J. Liu, Q. Fan, K. Wang, D. Luo and X. W. Sun, Circularly Polarized Luminescence from Semiconductor Quantum Rods Templated by Self-Assembled Cellulose Nanocrystals, *Journal of Materials Chemistry C*, 2020, **8**, 1048-1053.
14. X. Wang, J. Hao, J. Cheng, J. Li, J. Miao, R. Li, Y. Li, J. Li, Y. Liu, X. Zhu, Y. Liu, X. W. Sun, Z. Tang, M.-H. Delville, T. He and R. Chen, Chiral CdSe nanoplatelets as an ultrasensitive probe for lead ion sensing, *Nanoscale*, 2019, **11**, 9327-9334.
15. T. He, X. Qiu, J. Li, G. Pang, Z. Wu, J. Cheng, Z. Zhou, J. Hao, H. Liu, Y. Ni, L. Li, X. Lin, W. Hu, K. Wang and R. Chen, Water-Soluble Chiral CdSe/CdS Dot/Rod Nanocrystals for Two-Photon Fluorescence Lifetime Imaging and Photodynamic Therapy, *Nanoscale*, 2019, **11**, 15245-15252.
16. X. Qiu, J. Hao, J. Li, Z. Gong, S. Li, J. Cheng, X. Lin and T. He, Strong Multiphoton Absorption In Chiral CdSe/CdS Dot/Rod Nanocrystal-Doped Poly(Vinyl Alcohol) Films, *Optics Letters*, 2019, **44**, 2256-2259.
17. F. Purcell-Milton, A. K. Visheratina, V. A. Kuznetsova, A. Ryan, A. O. Orlova and Y. K. Gun'ko, Impact of Shell Thickness on Photoluminescence and Optical Activity in Chiral CdSe/CdS Core/Shell Quantum Dots, *ACS Nano*, 2017, **11**, 9207-9214.
18. A. B. Moshe and G. Markovich, Chiral Ligand-Induced Circular Dichroism in Excitonic Absorption of Colloidal Quantum Dots, *Isr. J. Chem.*, 2012, **52**, 1104-1110.

Please do not adjust margins

19. Y. Zhou, Z. Zhu, W. Huang, W. Liu, S. Wu, X. Liu, Y. Gao, W. Zhang and Z. Tang, Optical Coupling Between Chiral Biomolecules and Semiconductor Nanoparticles: Size-Dependent Circular Dichroism Absorption, *Angew. Chem. Int. Ed.*, 2011, **50**, 11456-11459.
20. J. K. Choi, B. E. Haynie, U. Tohgha, L. Pap, K. W. Elliott, B. M. Leonard, S. V. Dzyuba, K. Varga, J. Kubelka and M. Balaz, Chirality Inversion of CdSe and CdS Quantum Dots without Changing the Stereochemistry of the Capping Ligand, *ACS Nano*, 2016, **10**, 3809-3815.
21. M. V. Mukhina, I. V. Korsakov, V. G. Maslov, F. Purcell-Milton, J. Govan, A. V. Baranov, A. V. Fedorov and Y. K. Gun'ko, Molecular Recognition of Biomolecules by Chiral CdSe Quantum Dots, *Scientific Reports*, 2016, **6**, 24177.
22. J. Kuno, T. Kawai and T. Nakashima, The effect of surface ligands on the optical activity of mercury sulfide nanoparticles, *Nanoscale*, 2017, **9**, 11590-11595.
23. M. Puri and V. E. Ferry, Circular Dichroism of CdSe Nanocrystals Bound by Chiral Carboxylic Acids, *ACS Nano*, 2017, **11**, 12240-12246.
24. K. Varga, S. Tannir, B. E. Haynie, B. M. Leonard, S. V. Dzyuba, J. Kubelka and M. Balaz, CdSe Quantum Dots Functionalized with Chiral, Thiol-Free Carboxylic Acids: Unraveling Structural Requirements for Ligand-Induced Chirality, *ACS Nano*, 2017, **11**, 9846-9853.
25. G. Yang, M. Kazes and D. Oron, Chiral 2D Colloidal Semiconductor Quantum Wells, *Adv. Funct. Mater.*, 2018, **28**, 1802012.
26. X. Gao, B. Han, X. Yang and Z. Tang, Perspective of Chiral Colloidal Semiconductor Nanocrystals: Opportunity and Challenge, *Journal of the American Chemical Society*, 2019, **141**, 13700-13707.
27. X. Gao, X. Zhang, K. Deng, B. Han, L. Zhao, M. Wu, L. Shi, J. Lv and Z. Tang, Excitonic Circular Dichroism of Chiral Quantum Rods, *J. Am. Chem. Soc.*, 2017, **139**, 8734-8739.
28. J. Hao, Y. Li, J. Miao, R. Liu, J. Li, H. Liu, Q. Wang, H. Liu, M.-H. Delville, T. He, K. Wang, X. Zhu and J. Cheng, Ligand-Induced Chirality in Asymmetric CdSe/CdS Nanostructures: A Close Look at Chiral Tadpoles, *ACS Nano*, 2020, **14**, 10346-10358.
29. I. V. Martynenko, A. S. Baimuratov, V. A. Osipova, V. A. Kuznetsova, F. Purcell-Milton, I. D. Rukhlenko, A. V. Fedorov, Y. K. Gun'ko, U. Resch-Genger and A. V. Baranov, Excitation Energy Dependence of the Photoluminescence Quantum Yield of Core/Shell CdSe/CdS Quantum Dots and Correlation with Circular Dichroism, *Chem. Mater.*, 2018, **30**, 465-471.
30. S. Huo, P. Duan, T. Jiao, Q. Peng and M. Liu, Self-Assembled Luminescent Quantum Dots To Generate Full-Color and White Circularly Polarized Light, *Angew. Chem. Int. Ed.*, 2017, **56**, 12174-12178.
31. J. Yan, W. Feng, J.-Y. Kim, J. Lu, P. Kumar, Z. Mu, X. Wu, X. Mao and N. A. Kotov, Self-Assembly of Chiral Nanoparticles into Semiconductor Helices with Tunable near-Infrared Optical Activity, *Chem. Mater.*, 2020, **32**, 476-488.
32. S. J. Lim, W. Kim and S. K. Shin, A Photoetching-After-Growth Approach for the Synthesis of Nanocrystal Heterostructures Exhibiting Tunable Dual-Band Emission, *Adv. Mater. Interfaces*, 2020, **7**, 1901769.
33. H. Qin, Y. Niu, R. Meng, X. Lin, R. Lai, W. Fang and X. Peng, Single-Dot Spectroscopy of Zinc-Blende CdSe/CdS Core/Shell Nanocrystals: Nonblinking and Correlation with Ensemble Measurements, *Journal of the American Chemical Society*, 2014, **136**, 179-187.
34. B. N. Pal, Y. Ghosh, S. Brovelli, R. Laocharoensuk, V. I. Klimov, J. A. Hollingsworth and H. Htoon, 'Giant' CdSe/CdS Core/Shell Nanocrystal Quantum Dots As Efficient Electroluminescent Materials: Strong Influence of Shell Thickness on Light-Emitting Diode Performance, *Nano Letters*, 2011, **12**, 331-336.
35. W. Ma, J. Mao, C. Hao, L. Xu, C. Xu and H. Kuang, Chiral Semiconductor Nanorod Heterostructures with High Photocatalysis Activity, *Applied Catalysis B: Environmental*, 2019, **245**, 691-697.
36. W. Guo, J. J. Li, Y. A. Wang and X. Peng, Luminescent CdSe/CdS Core/Shell Nanocrystals in Dendron Boxes: Superior Chemical, Photochemical and Thermal Stability, *Journal of the American Chemical Society*, 2003, **125**, 3901-3909.
37. W. W. Yu, L. Qu, W. Guo and X. Peng, Experimental Determination of the Extinction Coefficient of CdTe, CdSe, and CdS Nanocrystals, *Chemistry of Materials*, 2003, **15**, 2854-2860.
38. L. Liu, Q. Peng and Y. Li, Preparation of CdSe Quantum Dots with Full Color Emission Based on a Room Temperature Injection Technique, *Inorganic Chemistry*, 2008, **47**, 5022-5028.
39. T. Uematsu, H. Kitajima, T. Kohma, T. Torimoto, Y. Tachibana and S. Kuwabata, Tuning of the fluorescence wavelength of CdTe quantum dots with 2 nm resolution by size-selective photoetching, *Nanotechnology*, 2009, **20**, 215302.
40. S. J. Lim, W. Kim, S. Jung, J. Seo and S. K. Shin, Anisotropic Etching of Semiconductor Nanocrystals, *Chemistry of Materials*, 2011, **23**, 5029-5036.
41. J. Liu, D. M. Aruguete, J. R. Jinschek, J. Donald Rimstidt and M. F. Hochella, The non-oxidative dissolution of galena nanocrystals: Insights into mineral dissolution rates as a function of grain size, shape, and aggregation state, *Geochimica et Cosmochimica Acta*, 2008, **72**, 5984-5996.
42. D. V. Talapin, N. Gaponik, H. Borchert, A. L. Rogach, M. Haase and H. Weller, Etching of Colloidal InP Nanocrystals with Fluorides: Photochemical Nature of the Process Resulting in High Photoluminescence Efficiency, *The Journal of Physical Chemistry B*, 2002, **106**, 12659-12663.
43. E. Khon, K. Lambright, R. S. Khnayzer, P. Moroz, D. Perera, E. Butaeva, S. Lambright, F. N. Castellano and M. Zamkov, Improving the Catalytic Activity of Semiconductor Nanocrystals through Selective Domain Etching, *Nano Letters*, 2013, **13**, 2016-2023.
44. B. Blackman, D. M. Battaglia, T. D. Mishima, M. B. Johnson and X. Peng, Control of the Morphology of Complex Semiconductor Nanocrystals with a Type II Heterojunction, Dots vs Peanuts, by Thermal Cycling, *Chemistry of Materials*, 2007, **19**, 3815-3821.
45. B. Blackman, D. Battaglia and X. Peng, Bright and Water-Soluble Near IR-Emitting CdSe/CdTe/ZnSe Type-II/Type-I Nanocrystals, Tuning the Efficiency and Stability by Growth, *Chemistry of Materials*, 2008, **20**, 4847-4853.
46. D. Battaglia, B. Blackman and X. Peng, Coupled and Decoupled Dual Quantum Systems in One Semiconductor Nanocrystal, *Journal of the American Chemical Society*, 2005, **127**, 10889-10897.
47. W. Ma, L. Xu, A. F. de Moura, X. Wu, H. Kuang, C. Xu and N. A. Kotov, Chiral Inorganic Nanostructures, *Chem. Rev.*, 2017, **117**, 8041-8093.

Please do not adjust margins

Please do not adjust margins

48. H. Li, K. Wu, J. Lim, H.-J. Song and V. I. Klimov, Doctor-blade deposition of quantum dots onto standard window glass for low-loss large-area luminescent solar concentrators, *Nature Energy*, 2016, **1**, 16157.
49. I. L. Medintz, H. T. Uyeda, E. R. Goldman and H. Mattoussi, Quantum dot bioconjugates for imaging, labelling and sensing, *Nature materials*, 2005, **4**, 435-446.
50. S. Li, H. Liu, W. Chen, Z. Zhou, D. Wu, R. Lu, B. Zhao, J. Hao, L. Yang, H. Yang, R. Cai, B. Xu, K. Wang and X. W. Sun, Low reabsorption and stability enhanced luminescent solar concentrators based on silica encapsulated quantum rods, *Solar Energy Materials and Solar Cells*, 2020, **206**, 110321.
51. X. Gao, X. Zhang, L. Zhao, P. Huang, B. Han, J. Lv, X. Qiu, S.-H. Wei and Z. Tang, Distinct Excitonic Circular Dichroism between Wurtzite and Zincblende CdSe Nanoplatelets, *Nano Letters*, 2018, **18**, 6665-6671.
52. L. Carbone, C. Nobile, M. De Giorgi, F. D. Sala, G. Morello, P. Pompa, M. Hytch, E. Snoeck, A. Fiore, I. R. Franchini, M. Nadasan, A. F. Silvestre, L. Chiodo, S. Kudera, R. Cingolani, R. Krahne and L. Manna, Synthesis and Micrometer-Scale Assembly of Colloidal CdSe/CdS Nanorods Prepared by a Seeded Growth Approach, *Nano Lett.*, 2007, **7**, 2942-2950.
53. J. J. Li, Y. A. Wang, W. Guo, J. C. Keay, T. D. Mishima, M. B. Johnson and X. Peng, Large-Scale Synthesis of Nearly Monodisperse CdSe/CdS Core/Shell Nanocrystals Using Air-Stable Reagents *via* Successive Ion Layer Adsorption and Reaction, *Journal of the American Chemical Society*, 2003, **125**, 12567-12575.
54. S. Deka, A. Quarta, M. G. Lupo, A. Falqui, S. Boninelli, C. Giannini, G. Morello, M. De Giorgi, G. Lanzani, C. Spinella, R. Cingolani, T. Pellegrino and L. Manna, CdSe/CdS/ZnS Double Shell Nanorods with High Photoluminescence Efficiency and Their Exploitation As Biolabeling Probes, *Journal of the American Chemical Society*, 2009, **131**, 2948-2958.
55. N. Berova, P. L. Polavarapu, K. Nakanishi, R. W. Woody and Editors, *Comprehensive Chiroptical Spectroscopy, Volume 1: Instrumentation, Methodologies, and Theoretical Simulations*, John Wiley & Sons, Inc., 2012.
56. Z. Zhou, K. Wang, Z. Zhang, C. Zhang, H. Liu, Y. Zhang, Z. Wen, S. Li, J. Hao, B. Xu, S. J. Pennycook, K. L. Teo and X. W. Sun, Highly Polarized Fluorescent Film Based on Aligned Quantum Rods by Contact Ink-Jet Printing Method, *IEEE Photonics Journal*, 2019, **11**, 1-11.
57. J. L. Mohanan, I. U. Arachchige and S. L. Brock, Porous Semiconductor Chalcogenide Aerogels, *Science*, 2005, **307**, 397-400.
58. G. Menagen, D. Mocatta, A. Salant, I. Popov, D. Dorfs and U. Banin, Selective Gold Growth on CdSe Seeded CdS Nanorods, *Chemistry of Materials*, 2008, **20**, 6900-6902.
59. E. Yoskovitz, G. Menagen, A. Sitt, E. Lachman and U. Banin, Nanoscale Near-Field Imaging of Excitons in Single Heterostructured Nanorods, *Nano Letters*, 2010, **10**, 3068-3072.
60. L. Carbone, C. Nobile, M. De Giorgi, F. D. Sala, G. Morello, P. Pompa, M. Hytch, E. Snoeck, A. Fiore, I. R. Franchini, M. Nadasan, A. F. Silvestre, L. Chiodo, S. Kudera, R. Cingolani, R. Krahne and L. Manna, Synthesis and Micrometer-Scale Assembly of Colloidal CdSe/CdS Nanorods Prepared by a Seeded Growth Approach, *Nano Lett.*, 2007, **7**, 2942-2950.
61. S. A. Ivanov, A. Piryatinski, J. Nanda, S. Tretiak, K. R. Zavadil, W. O. Wallace, D. Werder and V. I. Klimov, Type-II Core/Shell CdS/ZnSe Nanocrystals: Synthesis, Electronic Structures, and Spectroscopic Properties, *Journal of the American Chemical Society*, 2007, **129**, 11708-11719.
62. K. Wu, L. J. Hill, J. Chen, J. R. McBride, N. G. Pavlopolous, N. E. Richey, J. Pyun and T. Lian, Universal Length Dependence of Rod-to-Seed Exciton Localization Efficiency in Type I and Quasi-Type II CdSe@CdS Nanorods, *ACS Nano*, 2015, **9**, 4591-4599.
63. N. G. Pavlopoulos, J. T. Dubose, Y. Liu, X. Huang, N. Pinna, M.-G. Willinger, T. Lian, K. Char and J. Pyun, Type I *vs.* Quasi-Type II Modulation in CdSe@CdS Tetrapods: Ramifications for Noble Metal Tipping, *CrystEngComm*, 2017, **19**, 6443-6453.
64. W. Nan, Y. Niu, H. Qin, F. Cui, Y. Yang, R. Lai, W. Lin and X. Peng, Crystal Structure Control of Zinc-Blende CdSe/CdS Core/Shell Nanocrystals: Synthesis and Structure-Dependent Optical Properties, *Journal of the American Chemical Society*, 2012, **134**, 19685-19693.
65. G. Li, X. Fei, H. Liu, J. Gao, J. Nie, Y. Wang, Z. Tian, C. He, J.-L. Wang, C. Ji, D. Oron and G. Yang, Fluorescence and Optical Activity of Chiral CdTe Quantum Dots in Their Interaction with Amino Acids, *ACS Nano*, 2020, **14**, 4196-4205.
66. M. L. Mastronardi, F. Maier-Flaig, D. Faulkner, E. J. Henderson, C. Kübel, U. Lemmer and G. A. Ozin, Size-Dependent Absolute Quantum Yields for Size-Separated Colloidally-Stable Silicon Nanocrystals, *Nano Letters*, 2012, **12**, 337-342.
67. X. Dai, Z. Zhang, Y. Jin, Y. Niu, H. Cao, X. Liang, L. Chen, J. Wang and X. Peng, Solution-Processed, High-Performance Light-Emitting Diodes Based on Quantum Dots, *Nature*, 2014, **515**, 96-99.
68. C. L. Choi, K. J. Koski, S. Sivasankar and A. P. Alivisatos, Strain-Dependent Photoluminescence Behavior of CdSe/CdS Nanocrystals with Spherical, Linear, and Branched Topologies, *Nano Letters*, 2009, **9**, 3544-3549.
69. D. V. Talapin, J. H. Nelson, E. V. Shevchenko, S. Aloni, B. Sadtler and A. P. Alivisatos, Seeded Growth of Highly Luminescent CdSe/CdS Nanoheterostructures with Rod and Tetrapod Morphologies, *Nano Lett.*, 2007, **7**, 2951-2959.

Please do not adjust margins

TOC

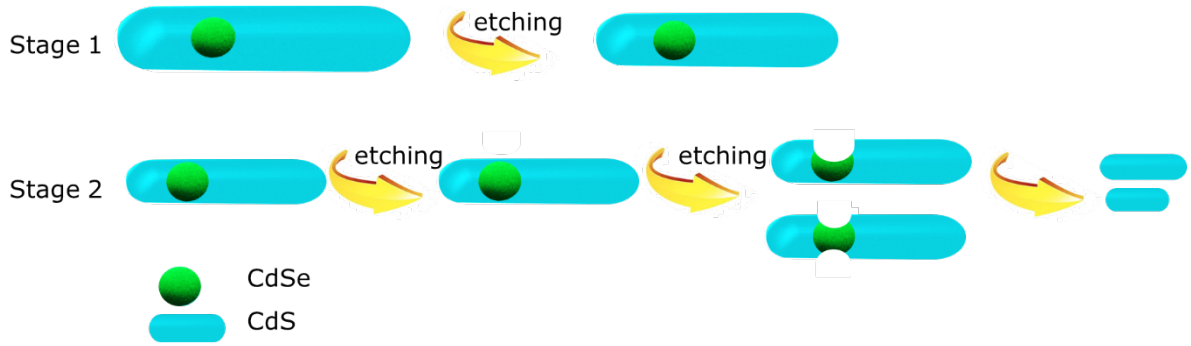

Please do not adjust margins